ARTICLE

Effect of Calcination Temperature on Surface Oxygen Vacancies and Catalytic Performance Towards CO Oxidation of Co_3O_4 Nanoparticles Supported on SiO_2

Jin-bing Li[a], Zhi-quan Jiang[b], Kun Qian[b], Wei-xin Huang[b*]

a. Yanshan Branch of SINOPEC Beijing Research Institute of Chemical Industry, Beijing 102500, China

b. Hefei National Laboratory for Physical Sciences at the Microscale, CAS Key Laboratory of Materials for Energy Conversion and Department of Chemical Physics, University of Science and Technology of China, Hefei 230026, China

(Dated: Received on September 20, 2011; Accepted on October 8, 2011)

Co_3O_4/SiO_2 catalysts for CO oxidation were prepared by conventional incipient wetness impregnation followed by calcination at various temperatures. Their structures were characterized with X-ray diffraction (XRD), laser Raman spectroscopy, X-ray photoelectron spectroscopy (XPS), temperature-programmed reduction (TPR) and X-ray absorption fine structure (XAFS) spectroscopy. Both XRD and Raman spectroscopy only detect the existence of Co_3O_4 crystallites in all catalysts. However, XPS results indicate that excess Co^{2+} ions are present on the surface of Co_3O_4 in $Co_3O_4(200)/SiO_2$ as compared with bulk Co_3O_4. Meanwhile, TPR results suggest the presence of surface oxygen vacancies on Co_3O_4 in $Co_3O_4(200)/SiO_2$, and XAFS results demonstrate that Co_3O_4 in $Co_3O_4(200)/SiO_2$ contains excess Co^{2+}. Increasing calcination temperature results in oxidation of excess Co^{2+} and the decrease of the concentration of surface oxygen vacancies, consequently the formation of stoichiometric Co_3O_4 on supported catalysts. Among all Co_3O_4/SiO_2 catalysts, $Co_3O_4(200)/SiO_2$ exhibits the best catalytic performance towards CO oxidation, demonstrating that excess Co^{2+} and surface oxygen vacancies can enhance the catalytic activity of Co_3O_4 towards CO oxidation. These results nicely demonstrate the effect of calcination temperature on the structure and catalytic performance towards CO oxidation of silica-supported Co_3O_4 catalysts and highlight the important role of surface oxygen vacancies on Co_3O_4.

Key words: Co_3O_4/SiO_2 catalyst, CO oxidation, Calcination temperature, Surface oxygen vacancies

I. INTRODUCTION

Low-temperature catalytic oxidation of CO has become an important research topic over the years in many environmental and industrial applications [1, 2]. The development of active and stable catalysts without noble metals for low-temperature CO oxidation under an ambient atmosphere remains a significant challenge. As a promising candidate of the substitute for precious metal catalysts, cobaltic oxides are very competitive and attractive for the presence of mobile oxygen on their surface [3−5]. Unsupported and supported cobaltic oxides have shown to be quite active for CO oxidation at low temperatures, even at temperatures below 0 °C [4−11]. Specially, Co_3O_4 nanorods with predominantly exposed {110} planes have been found to exhibit a very high activity for CO oxidation at −77 °C under normal conditions [12]. The most prevalent viewpoint is that Co_3O_4 is the active species for low-temperature CO oxidation over supported cobaltic oxide catalysts. Co_3O_4 has a spinel structure containing Co^{3+} in an octahedral coordination and Co^{2+} in a tetrahedral coordination, in ratio of 2:1 [13]. The former is regarded as the active site for CO oxidation, whereas the latter is almost inactive [8, 14, 15]. According to the results of X-ray diffraction (XRD), temperature-programmed reduction (TPR) and X-ray photoelectron spectroscopy (XPS), it was proposed that the finely dispersive CoO_x species with higher oxidation state on CoO_x/CeO_2 composite catalysts mainly contributed to their catalytic activity towards CO oxidation [16]. High-valence cobalt sites were also observed to contribute to the significant catalytic activity over other cobalt-oxide-containing catalysts towards CO oxidation [17−19]. However, bulk 3d

*Author to whom correspondence should be addressed. E-mail: huangwx@ustc.edu.cn, Tel.: +86-551-3600435, FAX: +86-551-3600437

transition metal oxides were examined as catalysts for preferential CO oxidation in the presence of excess H_2, in which bulk CoO catalyst showed the highest activity with a high selectivity over a wide temperature window [20]. It was also reported that the relative catalytic activity of bulk cobaltic oxides towards CO oxidation decreased significantly with the oxidation state of cobalt, *i.e.*, $CoO(+2) \geq Co_3O_4(+8/3) \gg CoO(OH)(+3) \geq$ high-valence cobalt oxide ($>+3$) [4, 5, 21]. Recently, ultrafine Co_3O_4-SiO_2 nanocomposites, whose surface is enriched with Co^{2+} species compared with normal Co_3O_4, were reported to exhibit a very high and quite stable activity for CO oxidation even at -76 °C [22]. Therefore, the valence state and local structure of the active center in supported and unsupported cobaltic oxide catalysts for low-temperature CO oxidation still remain controversial.

Final calcination temperature employed in the preparation of supported catalysts plays an important role in determining the dispersion, the physicochemical characteristics and the local structure of supported active component. The calcination temperature has been demonstrated to exert an impact on the dispersion of the cobaltic active species, which decreased with increasing calcination temperature [23, 24]. The chemical states of cobaltic oxide species were also correlated with the treatment conditions [25, 26]. In this work, the effect of calcination temperature on the surface physiochemical properties of Co_3O_4/SiO_2 catalysts has been investigated in detail by XRD, laser Raman spectroscopy, XPS, TPR, and X-ray absorption fine structure (XAFS) spectroscopy. Both XRD and Raman spectroscopy only detect crystalline Co_3O_4 in all Co_3O_4/SiO_2 catalysts. With respect to bulk Co_3O_4, excess Co^{2+} together with surface oxygen vacancies exists on the surface of Co_3O_4 in the catalyst calcined at 200 °C ($Co_3O_4(200)/SiO_2$). Further increasing calcination temperature leads to the formation of stoichiometric Co_3O_4 in the catalysts accompanied with agglomeration. The $Co_3O_4(200)/SiO_2$ catalyst exhibits the highest catalytic performance in CO oxidation, indicating that excess Co^{2+} and surface oxygen vacancies can enhance the catalytic activity of Co_3O_4 towards CO oxidation.

II. EXPERIMENTS

A. Catalyst preparation

Co_3O_4/SiO_2 catalysts were synthesized by conventional incipient wetness impregnation. The SiO_2 granules (20−50 mesh) were first calcined at 500 °C in air for 4 h prior to impregnation. The cobalt(II) nitrate hexahydrate, $Co(NO_3)_2{\cdot}6H_2O$, was dissolved in an appropriate volume of triply distilled water and then added to the silica support under stirring. The catalyst precursor was aged for 8 h at room temperature, and then dried in an oven at 80 °C for 6 h. Finally, the sample was transferred into a muffle furnace and calcined in air at the desired temperatures for 4 h. In this work, the cobalt loading was fixed at 6% in weight percentage. These catalysts were denoted as $Co_3O_4(y)/SiO_2$ catalysts, where y represented the final calcination temperature. For example, the $Co_3O_4(200)/SiO_2$ catalyst refers to the catalyst with 6% cobalt loading calcined at 200 °C.

B. Activity tests

The catalytic activities of Co_3O_4/SiO_2 catalysts towards CO oxidation were carried out in a continuous flow fixed-bed tubular micro-reactor at atmospheric pressure. The reaction gas, a mixture of dry air and 1%CO, was fed over a 50 mg catalyst at a flow rate of 20 mL/min. An on-line gas chromatograph (Shimadzu GC-14C) with a thermal conductivity detector (TCD) was employed to measure the constitutions of effluent gas streams. The chromatograph (H_2 as the carrier gas at 30 mL/min), equipped with a TDX-01 carbon sieve column, was operated with a column temperature of 80 °C and a TCD current of 100 mA. The conversion of CO was calculated from the change of CO concentrations in the inlet and outlet gases [27, 28].

C. Catalyst characterization

Powder XRD was performed at room temperature on a Philips X'Pert PRO SUPER X-ray diffractometer equipped with Ni-filtered Cu Kα radiation (λ=1.541874 Å). XPS measurements were carried out on a photoelectron spectrometer (Thermo Electron Corporation, ESCALAB 250) with an excitation source of nonmonochromatized Mg Kα ($h\nu$=1253.6 eV) and a pass energy of 20 eV. The binding energies in the XPS spectral analysis were corrected for specimen charging by referencing the Si2p in the silica support to 103.3 eV. Raman spectra were recorded under ambient conditions in a back-scattering configuration on a LABRAM-HR confocal laser Raman spectrometer, using 514.5 nm radiation from an argon ion laser. Thermogravimetric analysis (TGA) was performed on a Shimadzu TGA-50 analyzer, with the sample in an alumina crucible under synthetic airflow at a heating rate of 10 °C/min. Reduction behavior of Co_3O_4/SiO_2 catalysts was investigated by H_2-TPR. About 50 mg of the sample was heated in a flow of 10% H_2/He gas mixture at a flow rate of 10 mL/min. During TPR, the temperature was ramped from room temperature to 600 °C at 10 °C/min. A mass spectrometer (Hiden) was used for on-line monitoring of TPR effluent gas.

The XAFS spectra at the Co K-edge of Co_3O_4/SiO_2 catalysts were acquired at the U7C beamline of the National Synchrotron Radiation Laboratory (NSRL). The

DOI:10.1088/1674-0068/25/01/103-109

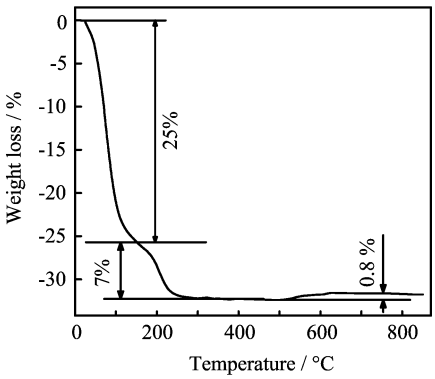

FIG. 1 TG profile in air flow for the $Co(NO_3)_2/SiO_2$ catalyst dried at 80 °C. Heating rate: 10 °C/min and air flow rate: 25 mL/min.

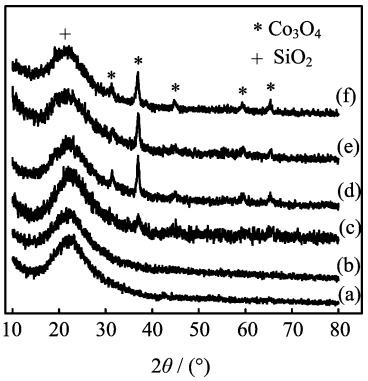

FIG. 2 XRD patterns of (a) SiO_2, (b) $Co(NO_3)_2/SiO_2$, and (c)−(d) Co_3O_4/SiO_2 catalysts calcined at (c) 200 °C, (d) 400 °C, (e) 600 °C, and (f) 700 °C.

storage ring of NSRL was operated at 0.8 GeV with a maximum current of 160 mA. The hard X-ray beam was from a three-pole superconducting Wiggler with a magnetic field intensity of 6 T. The fixed-exit Si(111) flat double crystals were used as monochromators. The XAFS spectra were recorded in a transmission mode with ionization chambers filled with Ar/N_2 at room temperature, using a Keithley Model 6517 Electrometer to collect the electron charge directly. The XAFS data were analyzed by UWXAFS3.0 [29] and USTCXAFS3.0 [30] software packages. The XANES (X-ray absorption near edge structure) spectra obtained after background correction were normalized by the edge height. For comparison, crystalline CoO and Co_3O_4 were used as standard compounds for the XANES analysis.

III. RESULTS AND DISCUSSION

Figure 1 displays the TG curve of the $Co(NO_3)_2/SiO_2$ precursor that was dried in air at 80 °C for 6 h after impregnation. An obvious weight loss of about 25% can be observed below 150 °C in the curve due to the loss of water. Another weight loss of about 7% over a temperature range from 150 °C to 250 °C could be attributed to thermal decomposition of $Co(NO_3)_2$. It indicates that prolonged calcination at 200 °C could lead to the complete decomposition of $Co(NO_3)_2$ impregnated on the silica support. Calcination at 200 °C for 4 h was therefore chosen as the mildest calcination condition for the preparation of Co_3O_4/SiO_2 catalysts. A small weight gain of about 0.8% arises in the temperature range of 500−650 °C, likely due to a deep oxidation of the cobaltic species. Bulk CoO is known to transform into Co_3O_4 by heating in air at temperatures of 400−500 °C, and CoO supported on alumina was observed to mainly convert to Co_3O_4 by calcination at 450 °C [31, 32]. Thus the weight increase of about 0.8% is attributed to the deep oxidation of the surface Co^{2+} component into Co^{3+}. Based on the weight loss of about 7% due to thermal decomposition of $Co(NO_3)_2$, this weight gain of about 0.8% is much less than the calculated value for the complete conversion of CoO to Co_3O_4, if assuming all surface species be CoO prior to the deep oxidation. Therefore, Co_3O_4 should dominate the silica-supported catalyst after calcination at 200 °C and $Co_3O_4(200)/SiO_2$ contains a very small portion of Co^{2+} that undergo the observed deep oxidation at elevated temperatures.

A series of Co_3O_4/SiO_2 catalysts were then prepared upon calcination at 200, 400, 600, and 700 °C. The XRD patterns of all samples are illustrated in Fig.2. The broad line centered at around $2\theta \approx 22°$ is due to the silica support. No diffraction pattern corresponding to the crystallized cobalt nitrate $Co(NO_3)_2 \cdot 6H_2O$ (JCPDS 18-425) could be observed in the XRD spectrum for $Co(NO_3)_2/SiO_2$ dried at 80 °C (Fig.2(b)), demonstrating a high dispersion of $Co(NO_3)_2$ on the silica support. The XRD spectrum of $Co_3O_4(200)/SiO_2$ (Fig.2(c)) gives weak diffraction peaks that can be indexed to the spinel form of the Co_3O_4 oxide (JCPDS 42-1467). With the increase of calcination temperature, these peaks continuously grow and become narrower, and eventually distinct diffraction peaks arise at 31.3°, 36.9°, 44.7°, 59.4°, and 65.4° for $Co_3O_4(700)/SiO_2$, which can be all indexed to Co_3O_4 crystallites. No diffraction peaks for Co metal (JCPDS 15-806) or other cobaltic oxides (CoO: JCPDS 48-1719; Co_2O_3: JCPDS 2-770) are observed in any of the XRD patterns. These results agree with previous results in which the Co_3O_4 species was detected as the only species in Co_3O_4/SiO_2 catalysts calcined at 400−700 °C reported by Wang *et al.* [6]. The XRD results also demonstrate that supported Co_3O_4 crystallites undergo agglomeration with increasing calcination temperature. According to the Scherrer equation, the average crystalline size of Co_3O_4 particles is estimated to increase from 11.7 nm in $Co_3O_4(200)/SiO_2$ to 17 nm in $Co_3O_4(700)/SiO_2$.

The vibrational features of Co_3O_4/SiO_2 catalysts were investigated by means of laser Raman spec-

DOI:10.1088/1674-0068/25/01/103-109

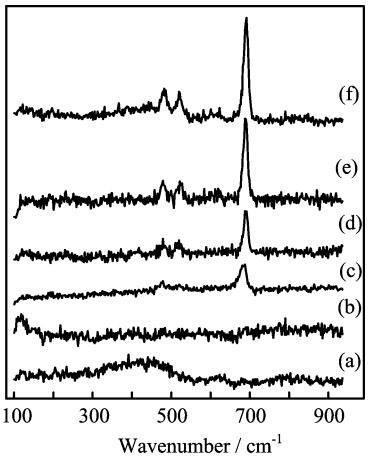

FIG. 3 Room temperature Raman spectra of (a) SiO_2, (b) $Co(NO_3)_2/SiO_2$, and (c)−(d) Co_3O_4/SiO_2 catalysts calcined at (c) 200 °C, (d) 400 °C, (e) 600 °C, and (f) 700 °C.

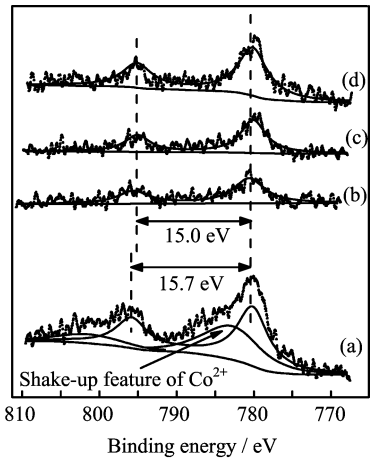

FIG. 4 Experimental (scatter) and deconvolved (solid line) Co2p XPS for Co_3O_4/SiO_2 catalysts calcined at (a) 200 °C, (b) 400 °C, (c) 600 °C, and (d) 700 °C.

troscopy, the results are shown in Fig.3. A broad Raman band between 200 and 570 cm^{-1} is present on the silica support, which is assigned to the silica support. This broad feature is suppressed upon $Co(NO_3)_2$ impregnation. However, no obvious Raman bands for $Co(NO_3)_2$ is observed on the $Co(NO_3)_2/SiO_2$ sample, which should exhibit vibrational features at 100−300 and 710−780 cm^{-1} [33]. This could be reasonably attributed to the high dispersion of $Co(NO_3)_2$ on the silica support, as observed by XRD. An intense Raman band at 686 cm^{-1} accompanied with a weak one between 410 and 590 cm^{-1} arises in the spectrum of $Co_3O_4(200)/SiO_2$. These bands on the catalysts grow with increasing calcination temperature, and eventually strong Raman bands develop at 691, 521, and 483 cm^{-1}, characteristic of crystalline Co_3O_4 [33]. Therefore, both XRD and Raman spectroscopy only detect crystalline Co_3O_4 in all supported catalysts.

The surface compositions of Co_3O_4/SiO_2 catalysts were studied by XPS, whose results are shown in Fig.4. Co^{2+} and Co^{3+} exhibit similar binding energies: 780.0 eV for Co^{3+} in CoOOH, 799.9 eV for Co^{3+} in Co_2O_3, and 780.0 eV for Co^{2+} in CoO [34], but they exhibit different satellite peaks and the spin-orbit splittings of the 2p level (ΔE). The concomitant difference of ΔE (15.0 eV for Co_3O_4, 15.7 eV for CoO) and the lineshape make it possible to distinguish Co^{2+} and Co^{3+} [35]. In addition, a shoulder at the high-energy side, which can be traced back to a shake-up process, can only be observed with Co^{2+} compounds in the high spin state whereas the diamagnetic low-spin Co^{3+} does not show any shake-up structures [36]. We made a quantitative analysis of Co2p XPS spectra by performing the peak fitting. The Co2p XPS for $Co_3O_4(200)/SiO_2$ shows the spin-orbital components of $Co2p_{3/2}$ and $Co2p_{1/2}$ at 780.1 and 795.8 eV, respectively, from which the ΔE was calculated to be 15.7 eV, which is characteristic of Co^{2+}, demonstrating that there are excess Co^{2+} existing on the surface of crystalline Co_3O_4 in $Co_3O_4(200)/SiO_2$. This is further supported by the prominent satellite structure in the Co2p XPS spectrum of $Co_3O_4(200)/SiO_2$. With the increase of calcination temperature, the $Co2p_{3/2}$ binding energy does not shift, but the separation (ΔE) due to the spin-orbit splitting of the 2p level decreases from 15.7 eV for $Co_3O_4(200)/SiO_2$ to 15.0 eV, meanwhile, the shake-up feature clearly visible in $Co_3O_4(200)/SiO_2$ disappears. These Co2p XPS features of Co_3O_4/SiO_2 catalysts caicined at 400 °C and higher temperatures are obviously characteristic of stoichiometric Co_3O_4. Although containing Co^{2+}, bulk Co_3O_4 only exhibits very weak satellite peak and only Co^{3+} characteristic appears in its Co2p XPS spectrum [37]. Therefore, XPS results demonstrate that Co_3O_4 in the Co_3O_4/SiO_2 catalyst calcined at 200 °C contains excess Co^{2+} on its surface while Co_3O_4 in the Co_3O_4/SiO_2 catalyst calcined at higher temperatures is stoichiometric. It is noteworthy that no N1s signal was detected by XPS in all Co_3O_4/SiO_2 catalysts, demonstrating the complete decomposition of $Co(NO_3)_2$ precursor.

It can be clearly seen that the Co2p XPS feature of $Co_3O_4(200)/SiO_2$ is significantly more intense than those of catalysts calcined at higher temperatures. With the same Co loading in all Co_3O_4/SiO_2 catalysts, the normalized intensity of the Co2p XPS peak is related with their dispersion. The much more intense Co2p XPS peak of $Co_3O_4(200)/SiO_2$ suggests a higher dispersion of cobaltic oxide species on SiO_2. The Co2p XPS intensity obviously decreases when the calcination temperature is increased from 200 °C up to 400 °C, indicating obvious agglomeration of supported Co_3O_4 occurs at 400 °C.

Both XRD and Raman spectroscopy detect the existence of sole Co_3O_4 species on SiO_2 in all supported

DOI:10.1088/1674-0068/25/01/103-109

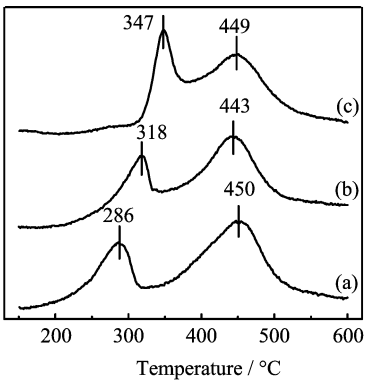

FIG. 5 H_2-TPR profiles of Co_3O_4/SiO_2 catalysts calcined at (a) 200 °C, (b) 400 °C, and (c) 700 °C.

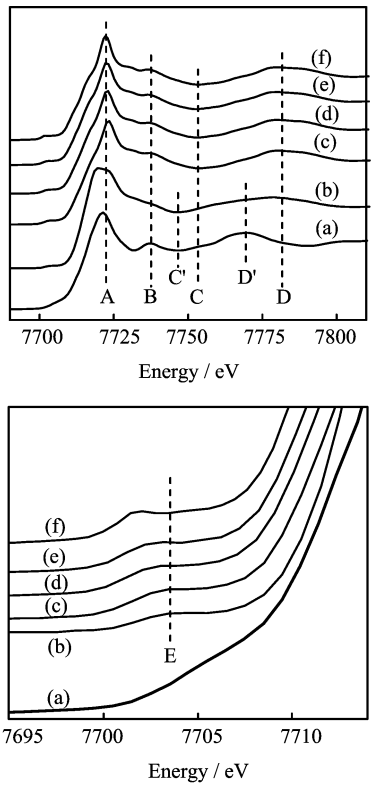

FIG. 6 Co K-edge XANES spectra of (a) CoO powder, (b) $Co_3O_4(200)/SiO_2$ catalyst, (c) $Co_3O_4(400)/SiO_2$ catalyst, (d) $Co_3O_4(600)/SiO_2$ catalyst, (e) $Co_3O_4(700)/SiO_2$ catalyst, and (f) Co_3O_4 powder.

catalysts. However, the XPS results indicate that excess Co^{2+} exist on the surface of $Co_3O_4(200)/SiO_2$, and the surface Co^{2+} component drastically decreases its intensity when the calcination temperature is increased from 200 °C up to 400 °C. As compared with bulk spinel Co_3O_4, it clearly suggests that there are surface oxygen vacancies present on $Co_3O_4(200)/SiO_2$. Therefore, the above results suggest that excess Co^{2+} and thus surface oxygen vacancies exist on the surface of Co_3O_4 in $Co_3O_4(200)/SiO_2$, but not in Co_3O_4/SiO_2 catalysts calcined at higher temperatures. The reducibility of Co_3O_4 in Co_3O_4/SiO_2 catalysts was then studied by TPR technique (Fig.5). All samples exhibit a similar TPR profile consisting of two well-resolved reduction peaks (denoted as α-peak at low temperature and β-peak at high temperature). Unsupported Co_3O_4 exhibited also two reduction peaks [38, 39]. According to the results in Refs. [4, 10, 16, 32, 36, 38−41], the low-temperature α-peak can be ascribed to the reduction of Co^{3+} into Co^{2+}, with the subsequent structural change to CoO, which followed the high-temperature β-peak due to the reduction of CoO to metallic cobalt. The β reduction peak of Co_3O_4/SiO_2 catalyst remains at almost the same temperature, but the α reduction peak shifts apparently towards higher temperature with the increase of calcination temperature. The reduction of Co^{3+} to Co^{2+} occurs at approximately 286 °C for $Co_3O_4(200)/SiO_2$, 318 °C for $Co_3O_4(400)/SiO_2$, and 347 °C for $Co_3O_4(700)/SiO_2$. This could be attributed to the following factors: (i) the surface of Co_3O_4 in $Co_3O_4(200)/SiO_2$ contains more surface oxygen vacancies than those in $Co_3O_4(400)/SiO_2$ and $Co_3O_4(700)/SiO_2$. It was observed that Co_3O_4 with more surface oxygen vacancies in CeO_2/Co_3O_4 catalysts was reduced at lower temperatures [10]. (ii) Co_3O_4 in $Co_3O_4(200)/SiO_2$ is finer than those in $Co_3O_4(400)/SiO_2$ and $Co_3O_4(700)/SiO_2$. It was reported that a small particle size can promote the desorption of lattice oxygen from Co_3O_4 to decrease the reduction temperature [4, 10].

We further employed XAFS to study the local structures of Co_3O_4/SiO_2 catalysts. XAFS has long been recognized as a powerful tool for determining the local structure of solid materials [42] because of its sensitivity to the short-range order and atomic species surrounding the absorbed atom. In addition, XANES spectroscopy can also be employed to distinguish the electronic structure of absorbed atom in condensed matters [43]. Figure 6 shows the Co K-edge XANES spectra of all Co_3O_4/SiO_2 catalysts. The spectrum for pure crystalline Co_3O_4 shows a pre-edge peak below the absorption edge which is assigned to the 1s→3d transition, and a sharp peak above the absorption edge derived from the 1s→4p transition (white line). The spectrum for pure crystalline CoO exhibits the corresponding white line and subsequent multiple scattering resonance but no pre-edge absorption peak. These features are consistent with that in Refs. [44−46]. The XANES spectra for all Co_3O_4/SiO_2 catalysts exhibit a strong absorption white line at approximately 7720 eV, with subsequent differences in the region above the absorption edge due to the existence of cobalt ions in different Co-O environments and oxidation states. Except for the $Co_3O_4(200)/SiO_2$ catalyst, other Co_3O_4/SiO_2 catalysts all exhibit the XANES characteristics very similar to that of pure crystalline Co_3O_4, both in the energy position and in the resonance intensity: the

DOI:10.1088/1674-0068/25/01/103-109

white line at position A, the shoulder at position B, the vale at position C, and the ridge at position D of the first resonance peak. Additionally, a distinct pre-edge peak emerges at position E in the XANES spectra for Co_3O_4/SiO_2 catalysts calcined at temperatures above 200 °C. These XANES features clearly prove that the local structures in Co_3O_4/SiO_2 catalysts calcined at temperatures above 200 °C are very close to those in crystalline Co_3O_4, in good accordance with the above XRD, Raman, and XPS results.

The XANES spectrum for $Co_3O_4(200)/SiO_2$ exhibits some characteristics of pure crystalline Co_3O_4, such as the absorption transition at 7.722 keV, the ridge at position D of the first resonance peak and the distinct pre-edge peak. However, several features similar to CoO also appear, for example, the vale at position C′ and a shoulder peak D′ in the spectrum of $Co_3O_4(200)/SiO_2$ are analogous to those of pure crystalline CoO. Therefore, XANES results indicate that Co_3O_4 in $Co_3O_4(200)/SiO_2$ catalyst exhibits more Co^{2+} characteristics than those in Co_3O_4/SiO_2 catalysts calcined at higher temperatures. That is to say, excess Co^{2+} ions exist on the surface of Co_3O_4 in $Co_3O_4(200)/SiO_2$, agreeing with the above XPS results.

The catalytic activities of Co_3O_4/SiO_2 catalysts towards CO oxidation are shown in Fig.7. The bare silica support is completely inactive in CO oxidation over the tested reaction temperature. All Co_3O_4/SiO_2 catalysts do not exhibit any activity at the reaction temperatures below 100 °C. With further increasing reaction temperature, the catalysts become active but their catalytic performances differ much. The catalytic activity towards CO oxidation of Co_3O_4/SiO_2 catalysts decreases with increasing calcination temperature. The $Co_3O_4(200)/SiO_2$ catalyst is the most active and achieves a 100% conversion of CO at 200 °C whereas the $Co_3O_4(700)/SiO_2$ catalyst only shows a maximum CO conversion of approximately 40% within the investigated reaction temperature region.

Although it decreases with the increase of calcination temperature, the dispersion of Co_3O_4 in Co_3O_4/SiO_2 catalysts can not solely explain their catalytic activity. For example, $Co_3O_4(200)/SiO_2$ and $Co_3O_4(400)/SiO_2$ exhibit a similar CO conversion at 150 °C, but achieve 100% and 35% conversion of CO at 200 °C, respectively. Therefore, the different catalytic activities of Co_3O_4/SiO_2 catalysts in CO oxidation should also be related with the structure of Co_3O_4. Co_3O_4 in Co_3O_4/SiO_2 catalysts calcined at elevated temperatures are stoichiometric but that in $Co_3O_4(200)/SiO_2$ is with excess Co^{2+} and surface oxygen vacancies on its surface. Co_3O_4 in $Co_3O_4(200)/SiO_2$ is also more easily to be reduced than those in Co_3O_4/SiO_2 catalysts calcined at higher temperatures. Therefore, these results indicate that excess Co^{2+} and surface oxygen vacancies can enhance the catalytic activity of Co_3O_4 supported on SiO_2 in CO oxidation. Very recently, it was reported that ultrafine Co_3O_4-SiO_2 nanocomposites with surface enriched with Co^{2+} species compared with normal Co_3O_4 exhibited a very high and quite stable activity for CO oxidation even at −76 °C [22]. Our results nicely demonstrate the effect of calcination temperature on the structure and catalytic performance towards CO oxidation of supported Co_3O_4 catalysts and highlight the important role of surface oxygen vacancies on Co_3O_4.

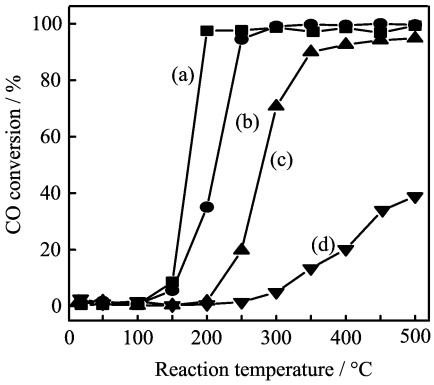

FIG. 7 CO conversion as a function of the reaction temperature over Co_3O_4/SiO_2 catalysts calcined at (a) 200 °C, (b) 400 °C, (c) 600 °C, and (d) 700 °C.

IV. CONCLUSION

$6\%Co_3O_4/SiO_2$ catalysts were prepared by incipient wetness impregnation using $Co(NO_3)_2{\cdot}6H_2O$ as the precursor followed by calcination at various temperatures and their catalytic activities towards CO oxidation were evaluated. The calcination temperature has a great influence on the dispersion and the local structure of Co_3O_4 species in Co_3O_4/SiO_2 catalysts. Compared with Co_3O_4/SiO_2 catalysts calcined at higher temperatures containing stoichiometric Co_3O_4 species, $Co_3O_4(200)/SiO_2$ contains Co_3O_4 with excess Co^{2+} on its surface, accompanied with surface oxygen vacancies. Excess Co^{2+} and surface oxygen vacancies can enhance the catalytic activity of Co_3O_4 supported on SiO_2 in CO oxidation. Among all catalysts, the $Co_3O_4(200)/SiO_2$ catalyst shows the best catalytic performance towards CO oxidation, achieving a 100% CO conversion at 200 °C. Our results nicely demonstrate the effect of calcination temperature on the structure and catalytic performance towards CO oxidation of supported Co_3O_4 catalysts and highlight the important role of surface oxygen vacancies on Co_3O_4.

V. ACKNOWLEDGMENTS

This work was supported by the National Natural Science Foundation of China (No.20803072, No.20973161, No.11079033), the Ministry of Science and Technol-

DOI:10.1088/1674-0068/25/01/103-109

ogy of China (No.2010CB923302), the Fundamental Research Funds for the Central Universities, Science and Technological Fund of Anhui Province for Outstanding Youth (No.2009SQRZ003ZD), and the MPG-CAS partner group program.

[1] M. F. Luo, J. M. Ma, J. Q. Lu, Y. P. Song, and Y. J. Wang, J. Catal. **246**, 52 (2007).
[2] B. K. Min and C. M. Friend, Chem. Rev. **107**, 2709 (2007).
[3] P. Broqvist, I. Panas, and H. Persson, J. Catal. **210**, 198 (2002).
[4] C. B. Wang, C. W. Tang, S. J. Gau, and S. H. Chien, Catal. Lett. **101**, 59 (2005).
[5] H. K. Lin, H. C. Chiu, H. C. Tsai, S. H. Chien, and C. B. Wang, Catal. Lett. **88**, 169 (2003).
[6] C. B. Wang, C. W. Tang, H. C. Tsai, and S. H. Chien, Catal. Lett. **107**, 223 (2006).
[7] J. Jansson, J. Catal. **194**, 55 (2000).
[8] J. Jansson, A. E. C. Palmqvist, E. Fridell, M. Skoglundh, L. Österlund, P. Thormählen, and V. Langer, J. Catal. **211**, 387 (2002).
[9] D. A. H. Cunningham, T. Kobayashi, N. Kamijo, and M. Haruta, Catal. Lett. **25**, 257 (1994).
[10] C. W. Tang, C. C. Kuo, M. C. Kuo, C. B. Wang, and S. H. Chien, Appl. Catal. A **309**, 37 (2006).
[11] M. Haruta, S. Tsubota, T. Kobayashi, H. Kageyama, M. J. Genet, and B. Delmon, J. Catal. **144**, 175 (1993).
[12] X. W. Xie, Y. Li, Z. Q. Liu, M. Haruta, and W. J. Shen, Nature **458**, 746 (2009).
[13] T. J. Chuang, C. R. Brundle, and D. W. Rice, Surf. Sci. **59**, 413 (1976).
[14] S. C. Petitto, E. M. Marsh, G. A. Carson, and M. A. Langell, J. Mol. Catal. A **281**, 49 (2008).
[15] K. Omata, T. Takada, S. Kasahara, and M. Yamada, Appl. Catal. A **146**, 255 (1996).
[16] M. Kang, M. W. Song, and C. H. Lee, Appl. Catal. A **251**, 143 (2003).
[17] P. Thormählen, M. Skoglundh, E. Fridell, and B. Andersson, J. Catal. **188**, 300 (1999).
[18] M. Meng, P. Y. Lin, and Y. L. Fu, Catal. Lett. **48**, 213 (1997).
[19] L. Simonot, F. Garin, and G. Maire, Appl. Catal. B **11**, 167 (1997).
[20] Y. Teng, H. Sakurai, A. Ueda, and T. Kobayashi, Intern. J. Hydrogen Energy **24**, 355 (1999).
[21] H. K. Lin, C. B. Wang, H. C. Chiu, and S. H. Chien, Catal. Lett. **86**, 63 (2003).
[22] C. J. Jia, M. Schwickardi, C. Weidenthaler, W. Schmidt, S. Korhonen, B. M. Weckhuysen, and F. Schüth, J. Am. Chem. Soc. **133**, 11279 (2011).
[23] R. L. Chin and D. M. Hercules, J. Phys. Chem. **86**, 360 (1982).
[24] S. W. Ho, M. Houalla, and D. M. Hercules, J. Phys. Chem. **94**, 6396 (1990).
[25] C. W. Tang, W. Y. Yu, C. J. Lin, C. B. Wang, and S. H. Chien, Catal. Lett. **116**, 161 (2007).
[26] A. Y. Khodakov, J. Lynch, D. Bazin, B. Rebours, N. Zanier, B. Moisson, and P. Chaumette, J. Catal. **168**, 16 (1997).
[27] K. Qian, Z. Q. Jiang, and W. X. Huang, J. Mol. Catal. A **264**, 26 (2007).
[28] K. Qian, W. X. Huang, Z. Q. Jiang, and H. X. Sun, J. Catal. **248**, 137 (2007).
[29] E. A. Stern, M. Newville, B. Ravel, Y. Yacoby, and D. Haskel, Physica B **208-209**, 117 (1995).
[30] W. J. Zhong, B. He, Z. Li, and S. Q. Wei, J. Chin. Univ. Sci. Technol. **31**, 328 (2001).
[31] L. Ji, J. Lin, and H. C. Zeng, J. Phys. Chem. B **104**, 1783 (2000).
[32] P. Arnoldy and J. A. Moulijn, J. Catal. **93**, 38 (1985).
[33] B. Jongsomjit, J. Panpranot, and J. G. Goodwin, J. Catal. **204**, 98 (2001).
[34] N. S. McIntyre and M. G. Cook, Anal. Chem. **47**, 2208 (1975).
[35] P. Konova, M. Stoyanova, A. Naydenov, S. Christoskova, and D. Mehandjiev, Appl. Catal. A **298**, 109 (2006).
[36] M. Voß, D. Borgmann, and G. Wedler, J. Catal. **212**, 10 (2002).
[37] Y. H. Zhang, H. F. Xiong, K. Y. Liew, and J. L. Li, J. Mol. Catal. A **237**, 172 (2005).
[38] B. Viswanathan and R. Gopalakrishnan, J. Catal. **99**, 342 (1986).
[39] B. A. Sexton, A. E. Hughes, and T. W. Turney, J. Catal. **97**, 390 (1986).
[40] H. Y. Lin and Y. W. Chen, Mater. Chem. Phys. **85**, 171 (2004).
[41] C. W. Tang, C. B. Wang, and S. H. Chien, Thermochim. Acta **473**, 68 (2008).
[42] E. D. Crozier, Physica B **208-209**, 330 (1995).
[43] J. J. Rehr and A. L. Ankudinov, Coord. Chem. Rev. **249**, 131 (2005).
[44] G. P. Huffman, N. Shah, J. M. Zhao, F. E. Huggins, T. E. Hoost, S. Halvorsen, and J. G. Goodwin, J. Catal. **151**, 17 (1995).
[45] J. S. Girardon, A. S. Lermontov, L. Gengembre, P. A. Chernavskii, A. Griboval-Constant, and A. Y. Khodakov, J. Catal. **230**, 339 (2005).
[46] A. M. Saib, A. Borgna, J. van de Loosdrecht, P. J. van Berge, J. W. Geus, and J. W. Niemantsverdriet, J. Catal. **239**, 326 (2006).

DOI:10.1088/1674-0068/25/01/103-109